Acta Pharmaceutica Sinica B 2025;15(11):6034−6051

Chinese Pharmaceutical Association
Institute of Materia Medica, Chinese Academy of Medical Sciences

Acta Pharmaceutica Sinica B

www.elsevier.com/locate/apsb
www.sciencedirect.com

ORIGINAL ARTICLE

A thermo-sensitive hydrogel targeting macrophage reprogramming for sustained osteoarthritis pain relief

Yue Liu[a,b,†], Kai Zhou[c,d,†], Xinlong He[c], Kun Shi[c], Danrong Hu[c], Chenli Yang[c], Jinrong Peng[c], Yuqi He[e], Guoyan Zhao[e], Yi Kang[e], Yujun Zhang[a,e], Yue'e Dai[b], Min Zeng[f], Feier Xian[f], Wensheng Zhang[a,e,*], Zhiyong Qian[c,*]

[a]*Department of Anaesthesiology, West China Hospital, Sichuan University, Chengdu 610041, China*
[b]*Department of Anaesthesiology, Sichuan Provincial People's Hospital, University of Electronic Science and Technology of China, Chengdu 610072, China*
[c]*State Key Laboratory of Biotherapy and Cancer Center, West China Hospital, Sichuan University, Chengdu 610041, China*
[d]*Department of Orthopedics and Orthopedic Research Institute, West China Hospital, Sichuan University, Chengdu 610041, China*
[e]*Laboratory of Anaesthesia and Critical Care Medicine, National-Local Joint Engineering Research Centre of Translational Medicine of Anaesthesiology, West China Hospital, Sichuan University, Chengdu 610041, China*
[f]*West China School of Medicine, West China Hospital, Sichuan University, Chengdu 610041, China*

Received 17 November 2024; received in revised form 20 February 2025; accepted 3 March 2025

KEY WORDS

Chronic pain;
Dorsal root ganglion;
Macrophages;
Osteoarthritis;
Thermo-sensitive hydrogel;
Neuroinflammation;
Drug delivery;

Abstract Osteoarthritis (OA) causes chronic pain that significantly impairs quality of life, with current treatments often proving insufficient and accompanied by adverse effects. Recent research has identified the dorsal root ganglion (DRG) and its resident macrophages as crucial mediators of chronic OA pain through neuroinflammation driven by macrophage polarization. We present a novel injectable thermo-sensitive hydrogel system, KAF@PLEL, designed to deliver an anti-inflammatory peptide (KAF) specifically to the DRG. This biodegradable hydrogel enables sustained KAF release, promoting the reprogramming of DRG macrophages from pro-inflammatory to anti-inflammatory phenotypes. Through comprehensive *in vitro* and *in vivo* studies, we evaluated the hydrogel's biocompatibility, effects on

*Corresponding authors.
E-mail addresses: zhang_ws@scu.edu.cn (Wensheng Zhang), anderson-qian@163.com (Zhiyong Qian).
[†]These authors made equal contributions to this work.
Peer review under the responsibility of Chinese Pharmaceutical Association and Institute of Materia Medica, Chinese Academy of Medical Sciences.

https://doi.org/10.1016/j.apsb.2025.07.024

Pain management

macrophage polarization, and therapeutic efficacy in chronic OA pain management. The system demonstrated significant capabilities in preserving macrophage mitochondrial function, suppressing neuroinflammation, alleviating chronic OA pain, reducing cartilage degradation, and improving motor function in OA rat models. The sustained-release properties of KAF@PLEL enabled prolonged therapeutic effects while minimizing systemic exposure and side effects. These findings suggest that KAF@PLEL represents a promising therapeutic approach for improving outcomes in OA patients through targeted, sustained treatment.

1. Introduction

Osteoarthritis (OA) affects over 7% of the global population, with a higher prevalence in developed countries[1]. This debilitating condition is characterized by chronic inflammation and persistent joint pain that significantly impairs quality of life and functional capacity[2,3]. As the disease progresses, pain often intensifies and becomes present even at rest, highlighting the substantial burden on affected individuals[4].

While OA pain has traditionally been attributed to joint injury and inflammation, as evidenced by the partial effectiveness of intra-articular injections and total joint replacement (TJR)[5−7], over 20% of patients continue to experience pain even after TJR[8−10]. This persistence of pain, coupled with the poor correlation between joint damage severity and pain intensity[11,12], suggests that pain mechanisms extend beyond localized inflammation. Recent preclinical and clinical studies increasingly recognize the role of central mechanisms in chronic OA pain development[13,14], particularly central sensitization, characterized by decreased pain thresholds, heightened pain responses, and impaired pain inhibition[15,16].

There are numerous methods for treating nerve-related pain. Commonly used intervention measures include neurodynamic treatment, pain neuroscience education, desensitization, exercise, physical agent modalities, mirror box therapy, kinesio taping, and targeted muscle reinnervation[17,18]. Despite common practice and anecdotal support, determining the appropriate intervention for each disease can be challenging. The dorsal root ganglion (DRG) has emerged as a critical site in OA pain processing, serving as an interface between the spinal cord and peripheral nerves[19]. The DRG comprises various cell types, including primary sensory neurons (PSN), satellite glial cells, Schwann cells, and resident immune cells, all contributing to pain modulation[20]. Notably, macrophages within the DRG accumulate during chronic pain conditions and adopt phenotypes that perpetuate pain through complex neuroimmune interactions[4,21,22]. Recent research has identified macrophage polarization in the DRG as a key contributor to chronic OA pain[22−24], with pro-inflammatory macrophages (M1) maintaining neuroinflammation by disrupting mitochondrial function and oxidative phosphorylation, thereby impeding their transition to an anti-inflammatory (M2) phenotype[25].

KAFAK (KAF), a cell-penetrating anti-inflammatory peptide, shows particular promise in this context through its inhibition of key pro-inflammatory cytokines, including IL-1, IL-6, and TNF-α, *via* modulation of mitogen-activated protein kinase-activated protein kinase 2 (MK2)[26−28]. Our previous research demonstrated KAF's effectiveness in promoting macrophage polarization toward the anti-inflammatory M2 phenotype[29]. In the present study, we first analyzed the gene expression omnibus (GEO) database of DRG to validate the critical role of neuroimmune mechanisms in chronic OA pain. Given the established biocompatibility, adaptability, and carrier capabilities of hydrogels[30], we developed an innovative KAF-loaded injectable hydrogel system, KAF@PLEL, based on a biodegradable thermo-sensitive hydrogel platform. This hydrogel utilizes the amphiphilic triblock copolymer poly(D,L-lactide)-poly (ethylene glycol)-poly(D,L-lactide) (PLEL), which has demonstrated exceptional biocompatibility and sustained drug delivery properties in our previous studies[31−33]. We present a comprehensive evaluation of KAF@PLEL, examining its biocompatibility, effects on macrophage polarization, and anti-inflammatory properties through both *in vitro* and *in vivo* OA models. Our findings demonstrate that KAF@PLEL effectively reduces microglial activation, mitigates neuroinflammation, and presents a promising new approach for chronic OA pain management.

2. Materials and methods

2.1. Materials

Poly(ethylene glycol) (PEG, Mn = 1500) was sourced from Nanjing Well Pharmaceutical Co., Ltd. (Nanjing, China). Stannous octoate ($Sn(Oct)_2$), acetonitrile, formic acid, and *o*-phthalaldehyde were procured from Sigma−Aldrich (St. Louis, MO, USA). D,L-Lactide (D,L-LA) was obtained from Jinan Daigang Biomaterial Co., Ltd. (Jinan, China). A CCK-8 kit was acquired from Oriscience Corp., Ltd. (Beijing, China). Promega (Beijing, China) provided a total RNA extraction kit. The cDNA synthesis kit was sourced from Bio-Rad (Hercules, CA, USA). Dulbecco's modified Eagle's medium (DMEM), penicillin−streptomycin, and fetal bovine serum (FBS) were purchased from Gibco (Grand Island, NY, USA). Cy5.5 was ordered from MedChemexpress (Monmouth Junction, NJ, USA). Isoflurane was supplied by RWD Life Science Co., Ltd. (Shenzhen, China). MIA and JC-1 kits were provided by Aladdin Biochemical Technology Co., Ltd. (Shanghai, China).

2.2. Animals

Sprague-Dawley rats (220 ± 20 g) were provided by Beijing HFK Bioscience, China. The animals were housed with ad libitum access to food and water in a controlled environment (22 °C, 12 h light/dark cycle). A 10-day adaptation period was allowed before the start of experiments. All procedures were conducted by the ethical guidelines for the care and use of laboratory animals as outlined by the U.S. National Institutes of Health (Publication No.

80−23, revised in 1996). The study was approved by the Committee of Animal Care at West China Hospital, Sichuan University, China (Approval No. 20230302054).

2.3. Bioinformatics analysis

The RNA expression profile dataset GSE140785 was downloaded from the GEO database. It provides comprehensive DRG transcriptional profiles during OA progression in a mouse DMM model and was selected for initial analysis. This dataset was chosen for its unique focus on DRG-specific changes and detailed characterization of neuroimmune interactions. While this dataset utilized a DMM model in mice, our subsequent validation studies were performed in a rat MIA model, as detailed previously. The complementary use of these models allows us to identify conserved mechanisms of OA pain across species and models. The R package limma was used to normalize data and conduct differential analysis (Bioconductor, v3.58.0, Seattle, WA, USA). Genes with $P < 0.05$ were considered as differentially expressed genes (DEGs). Gene ontology (GO) pathway enrichment analysis of DEGs was conducted and visualized by the "ClusterProfiler" package, and the cutoff criteria of "adjusted P value (Benjamini−Hochberg method), 0.05" was considered statistically significant. The PPI (Protein-Protein Interaction) network of related DEGs was further analyzed using the STRING database (Swiss Institute of Bioinformatics, v11.5, Lausanne, Switzerland), and the top 5% scores were identified as hub genes. The expressions of hub genes were statistically compared *via* the Mann−Whitney U test, and their expression in each sample was then visualized using the R package heatmap.

2.4. KAF@PLEL preparation

The PLEL was synthesized as previously described. In brief, PEG, D,L-LA, and $Sn(Oct)_2$ were combined in a dry glass flask under a nitrogen atmosphere and agitated at 140 °C for 12 h. The resulting copolymer was purified by washing with water at approximately 80 °C, followed by lyophilization to a constant weight and storage at −20 °C. The molecular weight of the PLEL copolymer was determined using gel permeation chromatography (GPC, Agilent 110 HPLC, Santa Clara, CA, USA).

The peptide KAF was synthesized using the Fmoc/PyBOP methodology. The Boc-Lys(Boc)-Merrifield resin was swollen in dichloromethane (DCM), and the BOC protection group was removed using a 10% TFA solution. The peptide grafting was performed on an automatic synthesizer, with Fmoc protective group removal conducted using a 30% hexahydropyridine solution in DMF. Peptide chains were cleaved from resins using a mixture of trifluoroacetic acid, phenol, water, ethyl dithiocarbamate, and methyl ethyl sulfide. The polypeptide was precipitated using cold ether, collected by centrifugation, and dried under a vacuum. The purification of peptides involved identification and collection using chromatography with a C18 reversed-phase column and mass spectrometry (Finnigan LCQ, Thermo Fisher Scientific Co., Ltd., San Jose, CA, USA). The optimal elution gradient was determined based on the peak time of the target peptide, and the peptide eluting peak was collected and freeze-dried.

PLEL was dissolved in PBS (pH = 8.0) at 4 °C with agitation (200 rpm) for 12 h to obtain a transparent solution. The concentration of PLEL was set at 20% based on injection resistance and release characteristics. KAF was added to the solution and stirred for an additional hour to obtain KAF@PLEL. The stability of KAF in the KAF@PLEL solution/hydrogel at 4 °C/37 °C was verified by determining the amount of KAF using HPLC on Days 3 and 7.

2.5. Dynamic rheological study of KAF@PLEL

The thermosensitive solution-hydrogel phase transition of KAF@PLEL was assessed using a rheometer (HAAKE Mars 60, Thermo Scientific, USA) with a parallel plate (20 mm diameter). The storage modulus (G') and loss modulus (G'') of KAF@PLEL with varying KAF concentrations (0.03%/0.1%/0.3%/1%/3%) in 20% PLEL were measured as a function of temperature from 20 °C to 50 °C at a heating rate of 2 °C/min. Data were collected at a frequency of 1.0 Hz and a controlled stress of 1 Pa. A 20% PLEL hydrogel was also tested for comparison.

2.6. Cell culture and CCK-8 assay

ND7/23 and C2C12 cells were used to evaluate the cytotoxicity of PLEL and KAF peptides on nerve and muscle cells *via* the CCK-8 assay. Cells were cultured in DMEM medium containing 10% FBS, 1% penicillin, and streptomycin at 37 °C in a humidified 5% CO_2 atmosphere. 1 mL of PLEL (20% wt) gel was encapsulated in a dialysis bag (8000 Da), and after successful gelation at 37 °C on a shaking incubator, it was immersed in 5 mL of PBS (37 °C) external solution. Subsequently, PBS external solution was collected on Day 1 or 3 for further experiments. Cells were seeded in 96-well plates at a density of 4000 cells/well and incubated for 24 h. The medium was then replaced with fresh medium containing PLEL hydrogel leachates (DMEM: leachate = 2:1) and/or KAF peptide. The CCK-8 assay was performed after an additional 48 h, and absorbance was measured at 450 nm using a microplate reader (Synergy Mx, Agilent Technologies Co., Ltd., Santa Clara, CA, USA). The relative viability of treated cells was calculated as a percentage of the untreated control group. Experiments were conducted in triplicate.

2.7. Quantitative real-time PCR

qPCR analyses were carried out with Bio-Rad CFX96 Real-Time PCR System (Hercules, CA, USA). We used the following primers: *IL-1β* forward: TgCCACCTTTTgACAgTgATg reverse: AAggTCCACgggAAAgACAC; *TNF-α* forward: CgAgTgACAA gCCTgTAgCC reverse: ACAAggTACAACCCATCggC; *IL-10* forward: CTgCTCTTACTgACTggCATgAg reverse: CA gCTggTCCTTTgTTTgAAAgA; *β-actin* forward: CATTgCTgA CAggATgCAgAAg reverse: TgCTggAAggTggACAgTgAgg. The relative expression level was calculated using the $2^{-\Delta\Delta CT}$ method. *β-actin* was used as the internal control for each sample.

2.8. Expression of IL-1β, TNF-α, and IL-10 by ELISA

To assess the impact of KAF peptide on cytokine expression in macrophages *in vitro*, we stimulated RAW264.7 cells with 100 ng/mL LPS for 24 h with or without KAF. After stimulation, medium samples were collected, and cells were washed to remove LPS. Cells were then cultured for an additional 24 h to capture macrophage-derived factors that could affect neurons. Then, ND7/23 cells were incubated with the supernatant with macrophage-derived factors for another 24 h. Thereafter, the ND7/23 cells were washed and further incubated for another 24 h. Subsequently, the culture medium samples were collected for

assay. The concentrations of cytokines IL-1β, TNF-α, and IL-10 were measured using ELISA kits (ABclonal Technology, Wuhan, China) according to the manufacturer's protocol.

2.9. Flow cytometric assays

The suspended RAW264.7 cells were fixed in 4% paraformaldehyde at room temperature for 15 min and washed with PBS containing 5% fetal bovine serum. Subsequently, the cells were resuspended in 100 μL PBS and immunostained with anti-CD86-PE (1:1000, Biolegend #105007) at 4 °C for 60 min. After the staining process, the cells were washed and loaded. The gating strategy can be found in Supporting Information Fig. S1A.

2.10. KAF release in vitro

The *in vitro* release of the peptide KAF was measured using a dialysis method. A 0.3% KAF@PLEL solution was added to dialysis tubes (MWCO = 8000, Yuanye, Shanghai, China) and incubated at 37 °C for 30 min to form a hydrogel. The tubes were then placed in centrifuge tubes containing 20 mL of 37 °C saline and shaken in an incubator at 37 °C. The released peptide solution was collected at predetermined intervals and replaced with fresh saline. The amount of released peptide was measured using an *o*-phthalaldehyde assay, with fluorescence intensity measured at 340 nm excitation and 455 nm emission using a Synergy Mx plate reader (Biotek Instruments, Inc., Winooski, VT, USA). Three replicate tests were conducted and averaged.

2.11. Drug release in vivo

To explore drug release from PLEL hydrogel *in vivo*, we injected Cy5.5 solution and Cy5.5@PLEL adjacent to the DRG (L3−5) on the right side of rats. Fluorescence imaging was performed at 1, 8, 24, and 48 h, Days 5, 7, and 14 post-injection using an IVIS Lumina III imaging system (PerkinElmer, Inc., Waltham, MA, USA).

2.12. Mitochondrial membrane potential assay

RAW264.7 cells and ND7/23 cells were seeded in 24-well plates at densities of 50,000 cells/well and allowed to grow for 24 h. Cells were treated with LPS (100 ng/mL) and/or KAF (70 μg/mL) for 6 h. The mitochondrial membrane potential was measured after a 20-min incubation with JC-1 (5 μmol/L). Cells were washed with PBS and trypsinized, and fluorescence was analyzed using flow cytometry (Cytoflex, Beckman Coulter, Inc., Brea, CA, USA). Mean fluorescence intensity values were expressed as fold changes relative to untreated cells.

2.13. Seahorse metabolic assay

RAW264.7 cells were seeded in 24-well plates at a density of 30,000 cells/well and allowed to grow for 24 h. Oxygen consumption rates (OCR) and extracellular acidification rates (ECAR) were measured using an XF 24 Analyzer (Seahorse Bioscience, Agilent Technologies Co., Ltd., Santa Clara, CA, USA). The assay protocol of 2 min mix, 2 min wait, and 3 min measure was repeated three times for baseline rates and after each injection. Injection ports contained oligomycin A (10 μmol/L), FCCP (0.5 μmol/L), rotenone with antimycin A (both at 1 μmol/L) for OCR measurement; glucose (5 mmol/L), oligomycin A (10 μmol/L), and 2-DG (50 mmol/L) for ECAR measurement.

2.14. Ultrasound-guided para-DRG injection

Based on previous research[34], we developed an ultrasound-guided para-DRG injection method to minimize injury (Supporting Information Fig. S2). In the positioning verification experiment, rats were euthanized with an overdose of pentobarbital sodium. After hair removal from the back, rats were positioned laterally prone. An ultrasonic probe (13−6 MHz, Sonosite, Inc., Bothell, WA, USA) was used to locate the intervertebral foramen by identifying the articular processes. A 26G needle was used to puncture and reach the intervertebral foramen, and 20 μL methylene blue was injected for localization. The intervertebral foramen was dissected to reveal DRG wrapped in methylene blue. In the following experiments, 100 μL KAF@PLEL was injected at each DRG according to this method under isoflurane anesthesia.

2.15. MIA-induced OA

MIA (1 mg) was injected into the right knee joint of each rat using a 30G needle. Control and saline groups received 50 μL saline solution. The injected fluid was confined to the joint cavity. Drug doses were based on preliminary experiments and literature[35,36].

2.16. KAF@PLEL administration

Male rats (n = 63) were randomly divided into seven groups following MIA injection: (1) OA, (2) Vehicle (PLEL), (3) 0.03% KAF@PLEL, (4) 0.1% KAF@PLEL, (5) 0.3% KAF@PLEL, (6) 1% KAF@PLEL, (7) 3% KAF@PLEL. Each group received three para-DRG injections on Days 1, 7, and 14 post-MIA. Another 18 male rats were divided into two groups: (1) Control, receiving 50 μL saline in the knee joint without para-DRG injection, and (2) Saline, receiving 50 μL saline in the knee joint and three para-DRG injections with saline.

2.17. Gait analysis

Gait analysis was conducted over 6 weeks, and rats were tested in random order. The VisuGait system (Xinruan Information Technology Co., Ltd., Shanghai, China) was used to measure gait. Rats walked on a glass plate, with paw prints captured by a high-speed camera as they touched the plate. The parameters of "max contact area", "swing speed", "contact time proportion", "walking velocity", and "stride length" were automatically determined by analyzing footprints. Evaluations were based on the difference in parameters between the right hind limb (MIA-injected side) and the left hind limb.

2.18. Von frey test

The mechanical withdrawal threshold was assessed using an electronic von Frey unit (Bioseb, France) on a metal mesh floor. The simulator touched the paw gently from below, raising it until the rat moved its paw or the maximum force was reached. Three measurements were taken at 30-min intervals and averaged.

2.19. RNA sequencing

Gene expression profiles of L3−5 DRGs from three control, OA, and 0.3% KAF@PLEL rats were determined using mRNA sequencing. Total RNA was extracted using TRIzol® Reagent, with quality assessed using a 5300 Bioanalyser (Agilent) and quantified using an ND-2000 (NanoDrop Technologies). High-quality RNA samples were used to construct sequencing libraries. mRNA was isolated and fragmented, and double-stranded cDNA was synthesized. The cDNA was subjected to end-repair, phosphorylation, and "A" base addition. Libraries were size-selected and PCR amplified. Paired-end RNA-seq libraries were sequenced using a NovaSeq 6000 sequencer (2 × 150 bp read length, Illumina, Inc., San Diego, CA, USA). Reads were aligned to the reference genome using HISAT2 software (Center for Computational Biology, Johns Hopkins University, Baltimore, MD, USA), and DEGs were identified using DESeq2. Functional enrichment analysis was performed using Goatools and KOBAS.

2.20. Histological and immunofluorescence analyses

Six weeks after MIA administration, the hearts, livers, spleens, lungs, kidneys, and the muscles adjacent to the injection sites and DRGs (L3−5) were collected and soaked in 4% PFA followed by 30% sucrose for H&E and immunofluorescence staining. The degree of inflammation of the muscle of each rat was scored by the blinded investigator by an established scoring standard[37,38]. Knee joints were dissected, fixed, and decalcified for safranin O fast green staining. Antibodies for IBA1 (#178846, Universal Biologicals, Cambridge, UK), DRP1 (#DF7037, Affinity Biosciences, Inc., Cincinnati, OH, USA), iNOS (#P29477, Universal Biologicals, Cambridge, UK), ATF-3 (#305293, Abcam plc, Cambridge, UK), and CGRP (#283568, Abcam plc, Cambridge, UK) were used for immunofluorescence labeling.

2.21. Statistical analysis

Data are presented as mean ± standard deviation (SD) and were analyzed using GraphPad Prism 10 software (GraphPad Software, Inc., La Jolla, CA, USA). Student's *t*-test was used for single comparisons between two groups, while one-way ANOVA was used for other data. A P-value <0.05 was considered statistically significant.

3. Results

3.1. Monocyte-macrophage involvement in DRG neuropathology of OA

Analysis of the GSE140785 dataset revealed 2056 differentially expressed genes (DEGs), comprising 1146 upregulated and 910 downregulated genes, following normalization that produced linear boxplot distributions (Fig. 1A and B). Gene ontology (GO) pathway analysis indicated these DEGs were involved in multiple biological processes, including myeloid cell differentiation, leukocyte migration, mononuclear cell proliferation, inflammatory response regulation, and neuroinflammatory processes (Fig. 1C).

Several key immune-related genes showed significant differential expression between Control and OA-DRG groups, including *CD40*, *CD274*, *Lyn*, *CD3e*, *Ptprc*, *Itgb2*, and *Itgam* (Fig. 1D and E). A heatmap analysis highlighted genes associated with immune activation and cell interactions, such as *Itgal*, *Itgam*, *Dock2*, *Nckap1L*, *Lyn*, *Itgb2*, *Rac2*, and *Ptpn6* (Fig. 1F). These genes regulate immune cell adhesion, migration, and signaling, suggesting significant involvement of monocyte-macrophage lineage cells in OA-related neuroinflammatory processes. These findings led us to investigate the role of macrophages in DRG neuroinflammation during OA progression.

3.2. Preparation and characterization of KAF@PLEL hydrogel

The PLEL hydrogel was synthesized through ring-opening copolymerization of D,L-LA, initiated by PEG, and catalyzed by Sn $(Oct)_2$. ^{1}H NMR spectrum (Fig. 2A) and Gel permeation chromatography (GPC) confirmed the successful synthesis of the PLEL triblock copolymer, demonstrating an unimodal molecular weight distribution with an average molecular weight of 5107 and a polydispersity index (PDI) of 1.66 (Fig. S1B). The hydrogel exhibited temperature-dependent phase transition, remaining liquid at room temperature and forming a semi-solid at body temperature. Increasing KAF peptide concentrations resulted in decreased pH values (from 6.4 to 3.6) and increased hydrogel transmittance at both 25 and 37 °C (Fig. 2B).

Dynamic rheological measurements assessed the mechanical properties of KAF@PLEL during sol-gel transition. All KAF@PLEL and blank PLEL formulations showed significant increases in storage modulus (G') with temperature, with a sharp increase around 30 °C indicating the sol-gel transition point (Fig. 2C). Notably, KAF peptide incorporation had minimal impact on the sol-gel transition temperature. The intersection points of storage modulus (G') and loss modulus (G'') are marked in Fig. 2C, with complete rheological mechanical profiles provided in Fig. S1C−S1H.

The stability of KAF@PLEL was evaluated by maintaining 1% KAF@PLEL hydrogel at 37 °C for 21 days. A progressive transition from semi-solid to gel state was observed over time (Fig. 2D), likely due to PLEL biodegradation. High-performance liquid chromatography (HPLC) analysis confirmed KAF peptide stability in KAF@PLEL at both 4 and 37 °C (Fig. 2E). These results demonstrate that KAF incorporation maintains the hydrogel's thermo-sensitive properties while ensuring stability for sustained drug release.

3.3. Cytotoxicity assessment and anti-inflammatory effects

The biocompatibility of KAF@PLEL hydrogel and KAF peptide was evaluated using ND7/23 nerve cells and C2C12 muscle cells. CCK-8 assays showed that PLEL hydrogel leachate exhibited minimal cytotoxicity toward ND7/23 cells, maintaining over 90% cell viability even after 48 h exposure to 3 days leachate (Fig. 2F). When cells were co-cultured with both PLEL leachate and KAF peptide for 48 h, cell viability remained above 80% for KAF concentrations between 3 and 100 μg/mL. However, at 300 μg/mL KAF, ND7/23 cell viability decreased to 66.7%. Similar trends were observed in C2C12 cells (Fig. 2G). Independent assessment of KAF peptide showed that high concentrations could inhibit cell activity (Fig. S1I). These results indicate suitable biocompatibility of both KAF peptide and PLEL for OA pain treatment applications.

The anti-inflammatory effects of the KAF peptide were examined in LPS-stimulated RAW264.7 macrophages. Quantitative PCR analysis revealed that LPS significantly increased mRNA expression of IL-1β (75.9-fold, Fig. 2Hi), TNF-α (6.3-fold,

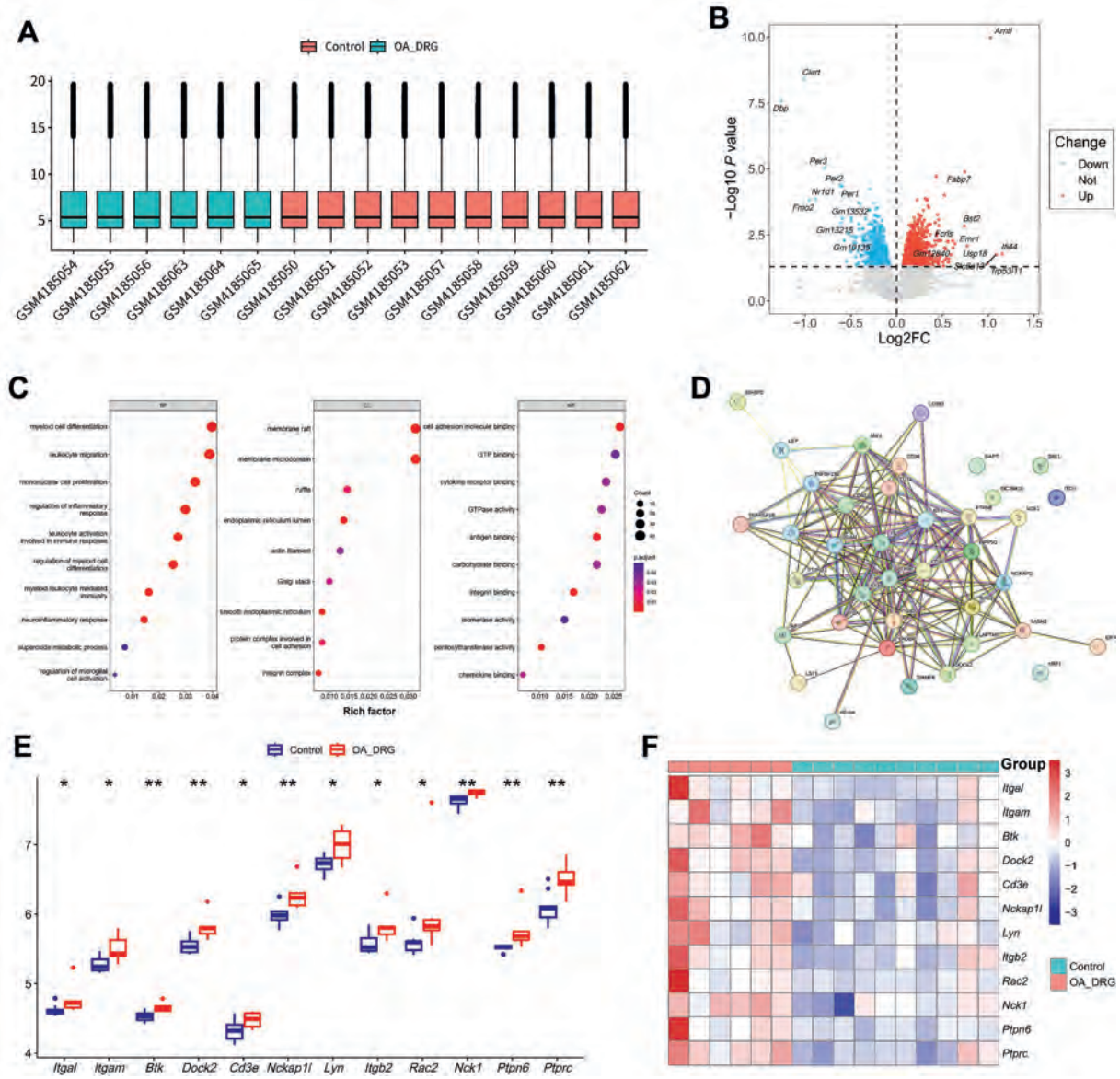

Figure 1 Gene expression analysis in osteoarthritis (OA) DRG progression. (A) Normalization and boxplot distribution of GSE140785. (B) Volcano plot of differentially expressed genes (DEGs). This volcano plot illustrates the dynamic landscape of DEGs identified in the DRG progression of OA. (C, D) Gene ontology (GO) pathway enrichment analysis and genes associated with mononuclear cell proliferation enriched by DEGs. (E) Validation of hub genes in GSE140785. Data are presented as mean ± SD. $^{*}P < 0.05$, $^{**}P < 0.01$. (F) Heatmap for the expression levels of hub genes among different samples.

Fig. 2Hii), and IL-10 (7.5-fold, Fig. 2Hiii) compared to untreated cells. KAF peptide treatment significantly suppressed IL-1β and TNF-α expression while enhancing IL-10 expression (2.0-fold *versus* LPS group).

ELISA measurements confirmed that KAF peptide significantly reduced pro-inflammatory cytokine secretion in LPS-stimulated cells. IL-1β levels decreased from 532.1 ± 37.9 pg/mL (LPS-stimulated) to 327.1 ± 38.4 pg/mL (KAF-treated), compared to control levels of 236.8 ± 37.6 pg/mL (Fig. 2Ii). Similar inhibition was observed for TNF-α (Fig. 2Iii). Conversely, the anti-inflammatory cytokine IL-10 increased significantly in KAF-treated cells (43.3 ± 14.3 pg/mL) compared to LPS-stimulated cells (18.6 ± 1.9 pg/mL, Fig. 2Iiii). In ND7/23 cells, culture with LPS-stimulated RAW264.7 cell supernatant increased IL-1β release, while KAF treatment during LPS stimulation significantly reduced this effect (Fig. S1J).

Flow cytometry analysis with anti-CD86 PE staining demonstrated that LPS stimulation significantly increased the proportion of $CD86^{+}$ cells (50.7 ± 5.1% *versus* 2.8 ± 1.2%, Fig. 2J and K), while KAF peptide treatment substantially reduced the number of $CD86^{+}$ cells (4.8 ± 0.7%). These findings collectively support the KAF peptide's anti-inflammatory efficacy in macrophages.

3.4. *Sustained release of KAF peptide via KAF@PLEL*

In vitro release studies under simulated physiological conditions showed distinct release profiles between free KAF and KAF@PLEL. Free KAF in PBS exhibited rapid release, with

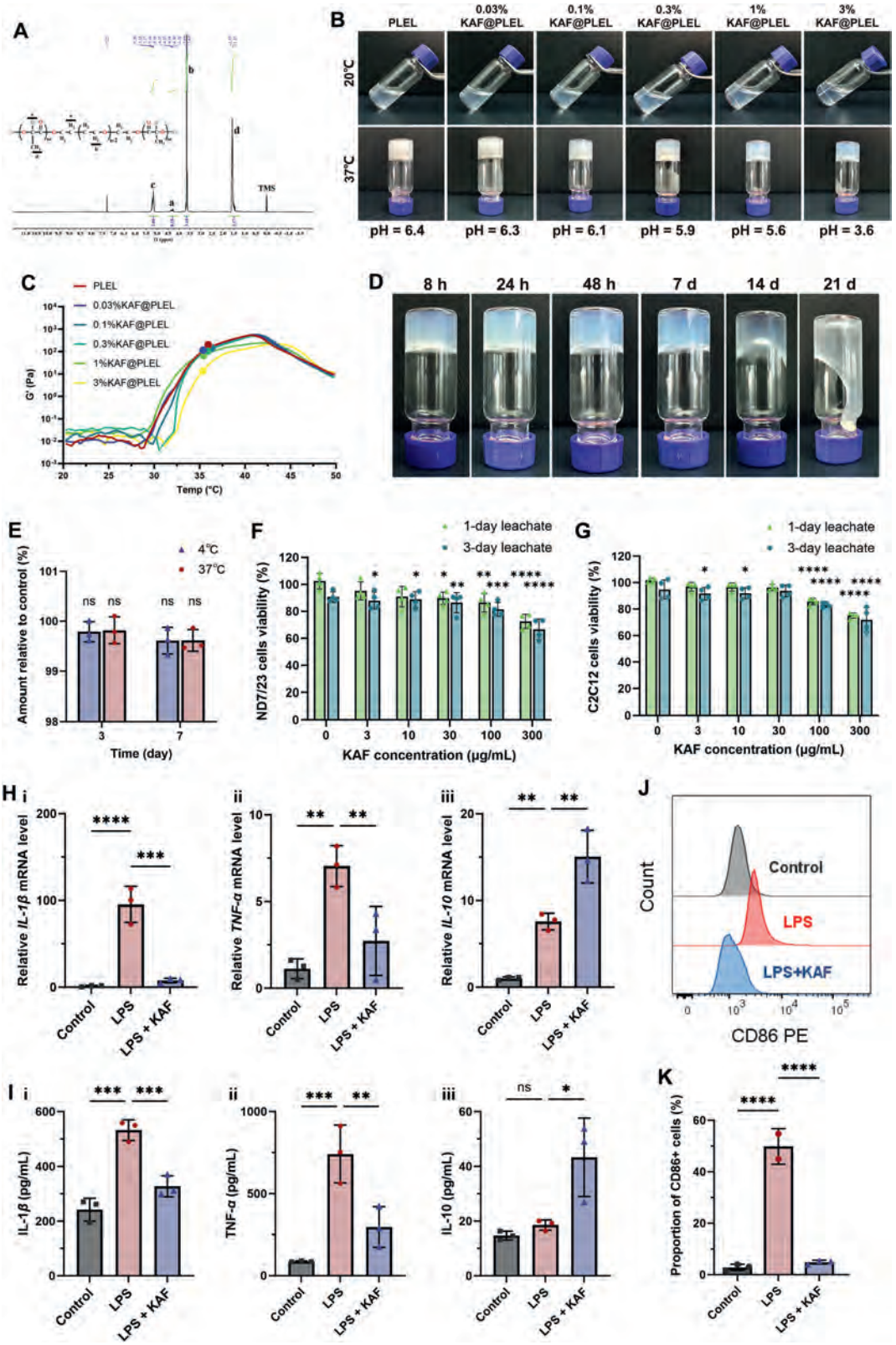

Figure 2 Characterization of KAF@PLEL hydrogel. (A) ^{1}H NMR spectrum of PLEL, illustrating the chemical composition. (B) Thermosensitivity and pH profiles of the blank PLEL hydrogel and the KAF peptide-loaded hydrogel, KAF@PLEL. (C) Dynamic rheological assessment of KAF@PLEL. The curves have been smoothed, and the dots indicate the intersection points when G′ is greater than G″. (D) The appearance changes of 1% KAF@PLEL upon time. (E) High-performance liquid chromatography (HPLC) analysis confirming the presence of KAF peptide within KAF@PLEL. Data are presented as mean ± SD (n = 3). ns, not significant compared with control. (F) Cytotoxicity evaluation of KAF peptide with PLEL hydrogel leachates on ND7/23 cell line after 48 h co-culture. Data are presented as mean ± SD (n = 4).

59.4% released within 24 h and complete release by 72 h. In contrast, KAF@PLEL demonstrated sustained release characteristics, with 15.4% released at 24 h, 47.3% at 72 h, continuing through 120 h (Fig. 3A). To visualize the hydrogel's sustained-release capabilities *in vivo*, we tracked Cy5.5 (as a KAF substitute) distribution in rats using an *in vivo* imaging system. Following injection of 3 × 100 μL Cy5.5 solution/hydrogel adjacent to L3−5 DRGs, the Cy5.5@PLEL group showed slower fluorescence decay compared to the Cy5.5 solution group, with fluorescence confined to the injection site (Fig. 3B). Quantitative analysis confirmed higher maintained fluorescence intensity at all time points in the Cy5.5@PLEL group (Fig. 3C).

The therapeutic efficacy of KAF@PLEL was assessed in OA rats using ultrasound-guided para-DRG injections of 1% free-KAF solution or 1% KAF@PLEL (20% hydrogel). While three weekly injections showed no significant effect on mechanical withdrawal threshold (MWT, Fig. 3D) in the first 15 days, KAF@PLEL effectively abolished mechanical hyperalgesia from Days 18−42 post monosodium iodoacetate (MIA), whereas free-KAF solution did not alleviate pain (Fig. 3E). The reduced efficacy in the free-KAF group likely reflects insufficient maintenance of effective concentrations in target nerve tissue. Following the final two injections (Days 7 and 14 post-MIA), the free-KAF group showed a slight, non-significant MWT decrease compared to controls. This effect may relate to the potential neurotoxicity of high KAF concentrations observed *in vitro*, as free drug formulations typically achieve higher peak tissue concentrations than sustained-release systems. These findings informed the design of subsequent optimization studies to determine optimal KAF@PLEL therapeutic concentrations.

3.5. KAF@PLEL promotes functional recovery and alleviates chronic pain

The restoration of function and pain relief were evaluated using gait analysis and von Frey tests (Fig. 4A). Considering the potential toxicity of high KAF concentrations, we systematically evaluated five concentrations of KAF@PLEL ranging from 0.03% to 3% to establish an optimal therapeutic window for OA pain treatment. A control group receiving saline para-DRG injections was included to assess delivery route safety.

To quantitatively assess treatment outcomes, Gait analysis was used to examine the impact of KAF@PLEL treatment on functional recovery in OA rats (Fig. 4B). Mechanical withdrawal threshold (MWT) testing was performed every three days until Day 30 post-MIA, followed by every four days until Day 42 (Fig. 4C). All groups displayed symmetrical gait parameters between ipsilateral (right) and contralateral (left) hind limbs before MIA injection (Supporting Information Fig. S3B, Supporting Information Fig. S4A and S4J), with no between-group differences in baseline MWT (Supporting Information Fig. S5A).

During the acute phase (Days 1−3 post-MIA, dpm), OA rats developed a decrease in the swing speed of the ipsilateral hind limb, with a compensatory increase in the swing speed of the contralateral hind limb (Fig. 4D, Fig. S4B and S4C). This asymmetry in swing speed between the two hind limbs marked the onset of the acute pain behavior. Similar asymmetric patterns were observed in the maximum contact area (Fig. 4E, Fig. S4K and S4L) and contact time proportion (Fig. S3A, S3C and S3D). Consistently with these gait alterations, the MWT showed rapid deterioration from 1 dpm (Fig. S5B).

While the acute phase differences in gait analysis were resolved by 7 dpm (Fig. S3E, Fig. S4D and S4M), mechanical hypersensitivity persisted until 18 dpm (Fig. S5D−S5H). Furthermore, rats in the saline group exhibited a transient reduction in MWT at 3 dpm (Fig. S5C), which returned to normal at 6 dpm (Fig. S5D). Rats that received blank PLEL hydrogel exhibited significantly reduced MWT from 3 to 9 dpm (Fig. S5C−S5E) compared to the OA group. These data suggest that both the para-DRG injection procedure and blank PLEL hydrogel may transiently affect mechanical sensitivity.

During the intermediate phase (7−21 dpm), gait differences in OA rats gradually normalized, except in the 3% KAF@PLEL group, which displayed persistent abnormal gait at 7, 14, and 21 dpm (Fig. S3E−S3G, Fig. S4D−S4F and Fig. S4M−S4O). These findings suggest that high concentrations of KAF peptide impaired the recovery of motor function.

The chronic phase (28−42 dpm) was characterized by renewed gait differences in OA rats. During this period, 0.1%, 0.3%, and 1% KAF@PLEL demonstrated significant therapeutic benefits on function restoration (Fig. S3H−S3J, Fig. S4G−S4I and Fig. S4P−S4R). Notably, abnormal gait in 3% KAF@PLEL rats resolved, with the gait analysis delta showing comparable values to the control. From 21 to 42 dpm, rats receiving 0.3% and 1% KAF@PLEL exhibited sustained elevation in MWT, indicating robust pain relief (Fig. S5I−S5O). Based on these behavioral assessments, 0.1%−1% KAF@PLEL emerged as the optimal therapeutic concentration range.

Longitudinal analysis of additional gait parameters revealed that walking velocity (Supporting Information Fig. S6A) and stride length (Fig. S6E) decreased throughout the observation period, with no significant differences between groups (Fig. S6B−S6D, S6F−S6H). Weekly monitoring of body weight showed no significant differences between groups (data not shown).

3.6. Effects of KAF@PLEL on neuroinflammation and macrophage polarization

To investigate the underlying mechanisms, we performed immunofluorescence staining on the ipsilateral L4 DRG of rats and analyzed at 42 days post-injury (Fig. 5A, overall view in Supporting Information Fig. S7). The intensity and size of DAPI-stained nuclei can be employed to discriminate PSNs from

$^{*}P < 0.05$, $^{**}P < 0.01$, $^{***}P < 0.001$, $^{****}P < 0.0001$. (G) Cytotoxicity assessment of KAF peptide with PLEL hydrogel leachates on C2C12 cell line following 48 h co-culture. Data are presented as mean ± SD ($n = 4$). $^{*}P < 0.05$, $^{****}P < 0.0001$. (H) qPCR analysis of IL-1β (i), TNF-α (ii), and IL-10 (iii) gene expression in the Raw264.7 cells stimulated with lipopolysaccharide (LPS), with or without KAF peptide treatment. Data are presented as mean ± SD ($n = 3$). $^{**}P < 0.01$, $^{***}P < 0.001$, $^{****}P < 0.0001$. (I) Enzyme-linked immunosorbent assay (ELISA) for IL-1β(i), TNF-α (ii), and IL-10(iii) cytokine levels in Raw264.7 cells stimulated with LPS, with or without KAF peptide treatment. Data are presented as mean ± SD ($n = 3$). $^{*}P < 0.05$, $^{**}P < 0.01$, $^{***}P < 0.001$. ns, not significant. (J) Fluorescence-activated cell sorting (FACS) evaluates the reversal of LPS-induced Raw264.7 cells differentiation by KAF peptide, utilizing anti-CD86 PE staining. (K) The proportion of $CD86^{+}$ Raw264.7 cells analyzed through FACS. Data are presented as mean ± SD ($n = 3$). $^{****}P < 0.0001$. ns, not significant.

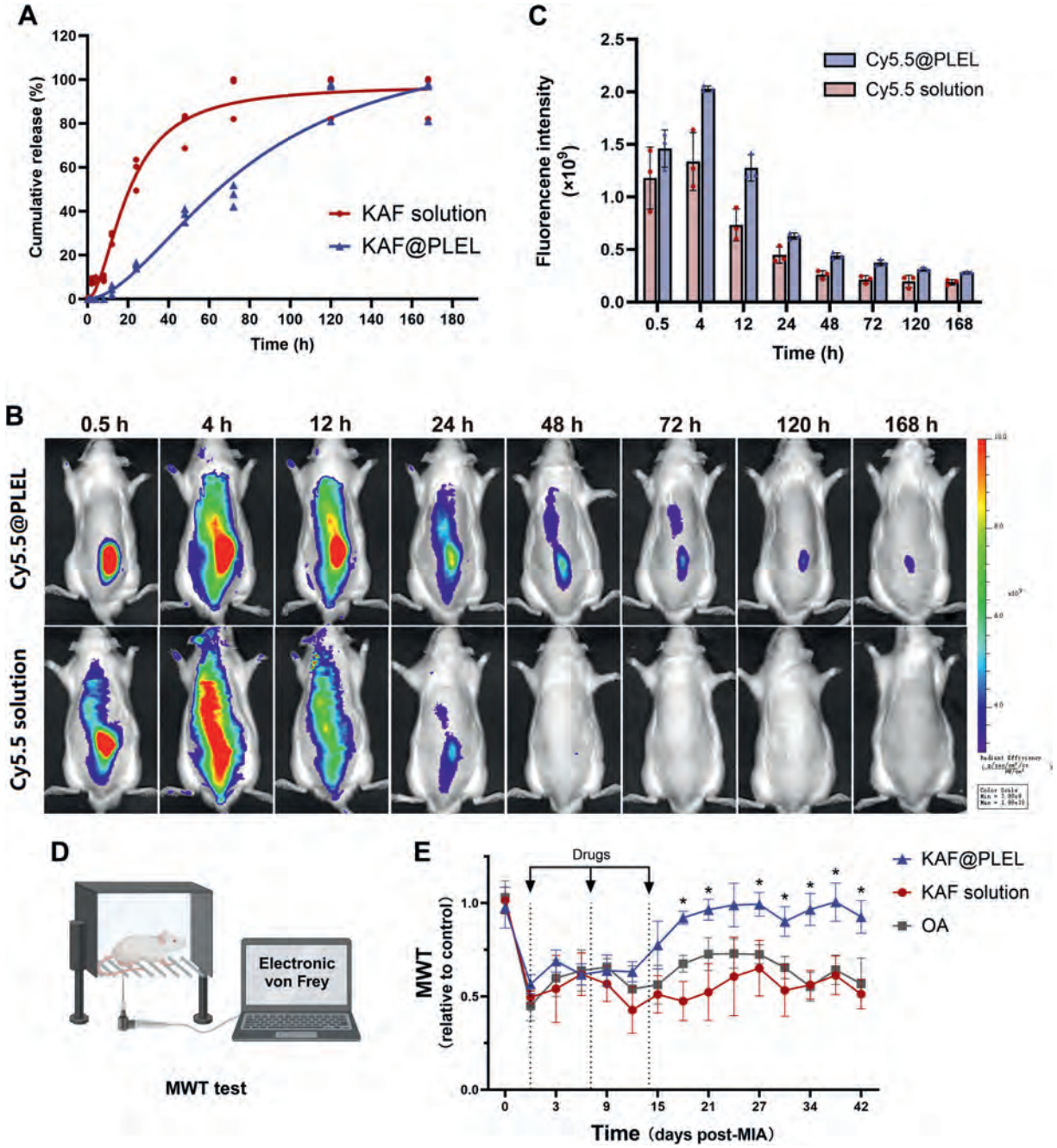

Figure 3 *In vitro*/*vivo* drug release and mechanical withdrawal threshold (MWT) assessment of KAF@PLEL. (A) *In vitro* release kinetics of KAF from KAF@PLEL hydrogel ($n = 3$). (B) Representative imaging and (C) quantitative analysis of Cy5.5 fluorescence intensity at various time points post-injection in rats, indicative of local drug retention ($n = 3$). (D) Schematic of the MWT test procedure. (E) Comparative MWT measurements in OA rats treated with KAF, KAF@PLEL, or saline. Data are presented as mean ± SD ($n = 4$). *$P < 0.05$.

surrounding residents and infiltrated immune cells. PSNs possess large and relatively weak nuclei, whereas immune cells have small and intensely stained nuclei. The DRG of OA animals exhibited significant DRP1 (a protein that promotes mitochondrial division in macrophages) expression surrounding PSNs, co-localizing with surrounding immune cells (Fig. 5Ai). As the concentration of KAF@PLEL increased, the fluorescence area of DRP1 decreased significantly when the concentration of KAF@PLEL reached 0.1%, and remained at a low level at higher concentrations (Fig. 5C). Similarly, the level of iNOS, a pro-inflammatory marker in macrophages (Fig. 5Aii), mirrored this trend but increased in the vehicle and 3% KAF@PLEL groups (Fig. 5D). This suggests that there may be additional mechanisms involved in the pro-inflammatory polarization of macrophages beyond DRP1.

Treatment with KAF@PLEL suppressed the expression of both ATF-3 (a sensitive marker for peripheral neuron injury, Fig. 5Aiii) and CGRP (a neuropeptide associated with neuroinflammatory pain, Fig. 5Aiv) in the PSNs of OA animals (Fig. 5E and F). Notably, the inhibitory effect was reduced in the 3% KAF@PLEL treated animals, suggesting potential nerve damage at higher KAF

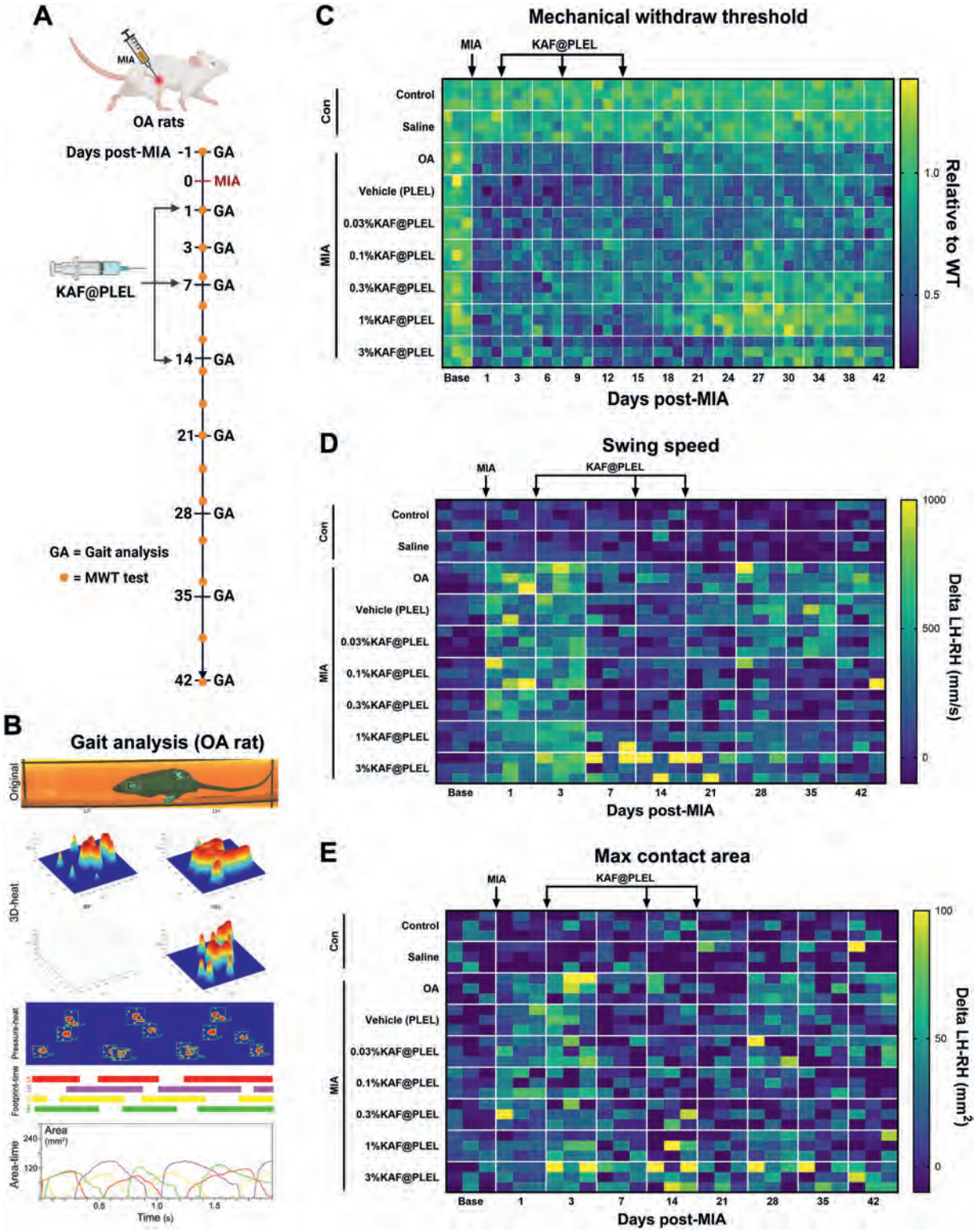

Figure 4 Restoration of motor function and analgesic efficacy in OA rats. (A) Schematic overview of the experimental protocol for OA induction and therapeutic intervention. (B) Gait analysis, including representative images and quantitative data, in an OA rat model. (C) Heatmap of the mechanical withdrawal threshold, as determined by the electronic von Frey test, normalized to the control group's average value. Each cube represents the data of an individual rat, whereas each larger rectangle (enclosing nine small cubes and delineated by a white line) corresponds to the data of a group on a specific day ($n = 9$). (D, E) Heatmaps depicting the swing speed and maximum contact area delta between left and right hind limbs, respectively, derived from gait analysis. Each cube represents the data of an individual rat, whereas each larger rectangle (enclosing nine small cubes and delineated by a white line) corresponds to the data of a group on a specific day ($n = 9$).

concentrations. Previous studies have shown a significant increase in reactive microglia around PSNs in OA and neurotoxicity animal models[39,40], where IBA1 serves as a hallmark protein for these cells. IBA1-positive microglial cells proliferated in the DRG of OA rats and surrounded PSN cells (Fig. 5Av). KAF@PLEL treatment at 0.1%, 0.3%, and 1% concentrations significantly inhibited IBA1-positive microglial proliferation, whereas the lowest (0.03%) and highest (3%) concentrations did not (Fig. 5G). In summary, KAF@PLEL can inhibit mitochondrial fission in OA animal DRG, reduce macrophage pro-inflammatory polarization, and protect PSN cells while suppressing microglial cell activation. However, at high concentrations, KAF@PLEL may have a detrimental effect on nerve cells and could potentially reactivate macrophage pro-inflammatory polarization and activate microglial cells through interactions between neurons and macrophages.

To assess cartilage destruction in the knee joint, we used safranin O/fast green staining to visualize cartilage and bone (Fig. 5B). In the OA and vehicle groups, the tidemark was absent, and the cartilage surfaces exhibited severe wear and degradation. In KAF@PLEL groups, as the concentration of KAF peptide increased, cartilage matrix erosion and tidemark loss were reduced, with greater preservation of proteoglycans. However, the protective effect of 3% KAF@PLEL on the joints was attenuated in comparison with that of lower concentrations of KAF@PLEL. Quantitative analysis of OA severity revealed that KAF@PLEL significantly reduced cartilage matrix loss (Fig. 5H) and Osteoarthritis Research Society International (OARSI) scores (Fig. 5I) in OA animals, indicating that KAF@PLEL treatment targeting DRG innervating the knee joint mitigated the OA damage process.

In consideration of the biosafety of injecting KAF@PLEL, we collected the heart, liver, spleen, lung, kidney, and muscle beside the injection site of rats for HE staining (Supporting Information Fig. S8A). No pathological alterations were detected in the HE sections of organs of the rats injected with KAF@PLEL. The muscle inflammation score indicated a mild infiltration of inflammatory cells in the muscles surrounding the injection site (Fig. S8B).

3.7. KAF protects mitochondria and aerobic metabolism of macrophages

The contribution of KAF to mitochondrial homeostasis was assessed using flow cytometry with JC-1 to quantify mitochondrial membrane potential. Results demonstrated that KAF peptide effectively maintained mitochondrial homeostasis in LPS-stimulated RAW264.7 cells (Fig. 6A). In contrast, while LPS stimulation did not significantly alter mitochondrial membrane potential in ND7/23 cells, the addition of KAF peptide led to decreased mitochondrial potential in these cells (Fig. 6B). Given neurons' high energy demands and reliance on mitochondrial oxidative phosphorylation for ATP production, these findings suggest KAF may exert an inhibitory effect on neuronal activity.

The impact of KAF peptide on cellular metabolism was examined in RAW264.7 cells using the Seahorse Mito-Stress Test and Glycolysis Stress Test, which evaluate oxygen consumption rate (OCR) and extracellular acidification rate (ECAR), respectively. OCR measurements in Fig. 6C enabled the determination of basal respiration (Fig. 6D), ATP production (Fig. 6E), non-mitochondrial oxygen consumption (Fig. 6F), and coupling efficiency (Fig. 6G). KAF peptide restored basal respiration and ATP production indices that were reduced by LPS, indicating recovery of LPS-suppressed oxidative phosphorylation (OXPHOS). ECAR analysis in Fig. 6H provided measurements of glycolysis (Fig. 6I), glycolytic capacity (Fig. 6J), glycolytic reserve (Fig. 6K), and non-glycolytic acidification (Fig. 6L). LPS addition increased basal glycolysis and glycolytic capacity in RAW264.7 cells. However, the KAF peptide did not significantly affect the increased glycolysis. We conclude that LPS-induced macrophages exhibit OXPHOS inhibition and increased glycolytic activity, while KAF peptide effectively prevents LPS-induced OXPHOS inhibition (Fig. 6M).

To identify transcriptomic changes associated with OA chronic pain treatment, RNA sequencing (RNA-seq) was performed on L3−5 DRGs from control, OA, and 0.3% KAF@PLEL-treated rats at 42 dpm. Hierarchical clustering and heat map analysis revealed distinct differences in the global transcriptomic landscape between the KAF@PLEL and OA groups (Fig. 7A). Using OA rats as a reference, we identified 865 upregulated and 171 down-regulated genes in the KAF@PLEL group (Fig. 7B, fold change ≥ 1.5; $P < 0.05$).

Gene ontology (GO) analysis of differential gene expression between KAF@PLEL-treated and OA rats revealed that KAF@PLEL treatment enhanced mitochondrial electron transfer and ATP generation (Fig. 7C). KEGG analysis showed up-regulation of oxidative phosphorylation in KAF@PLEL treated rats (Supporting Information Fig. S9A). Gene set enrichment analysis (GSEA) revealed up-regulation of mitochondrial membrane part and oxidative phosphorylation in KAF@PLEL treated rats (Fig. 7D and E), while both were down-regulated in OA rats compared with control rats (Fig. S9B and S9C). Additionally, neuroactive ligand−receptor interaction signaling appeared upregulated in OA rats (Fig. S9D), while it was down-regulated in KAF@PLEL and control groups (Fig. S9E). These results demonstrate that KAF@PLEL improves the decreased mitochondrial function in the DRG of OA rats and attenuates neuroactive interaction.

4. Discussion

Chronic pain development in osteoarthritis (OA) represents a complex interplay of peripheral joint damage, inflammation, and central sensitization mechanisms, with the dorsal root ganglion (DRG) serving as a critical nexus. Current pain management strategies, including conventional treatments such as NSAIDs, opioids, and local anesthetics, are limited by their side effects and inability to address the underlying neuroimmune mechanisms contributing to chronic pain[41,42]. Our newly developed KAF@PLEL hydrogel presents a promising solution that targets macrophage polarization and neuroinflammation in the DRG.

While our previous research established that PLEL-based hydrogels effectively prolonged analgesic effects in acute pain models[33], the control of neuroinflammation associated with chronic pain remained challenging. Traditional approaches, such as laminectomy and intrathecal injections, carry risks of motor function impairment, nerve injury, and systemic side effects[34,43,44]. For precise, minimally invasive DRG targeting, we developed an ultrasound-guided interventional injection technique. This approach offers a less invasive alternative, reducing risks while maintaining effective drug concentrations. Our method addresses the challenges of direct drug delivery to the DRG, which is anatomically challenging to reach due to its location beneath the vertebral lamina[45,46].

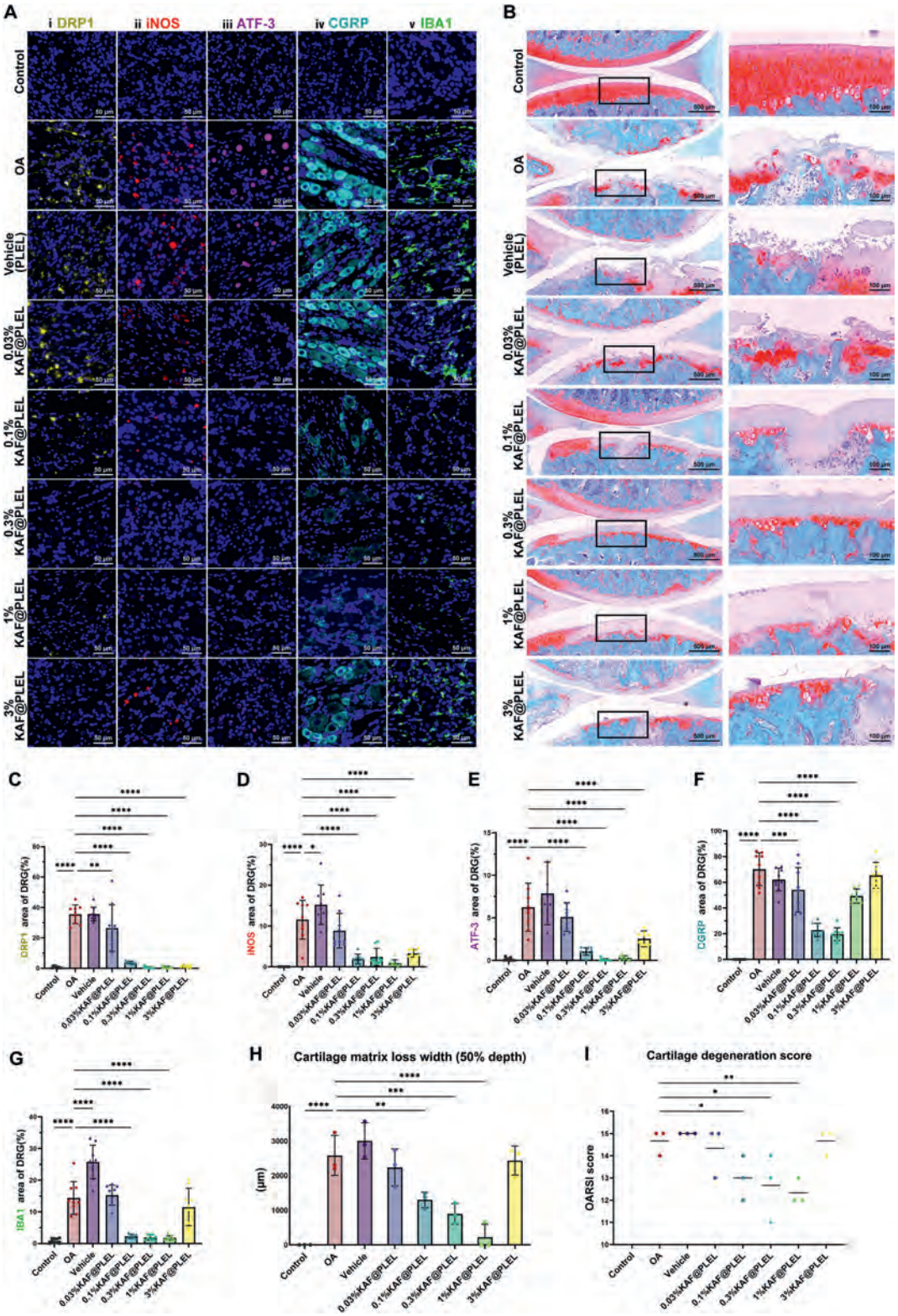

Figure 5 Histopathological evaluation on Day 42 post-MIA (dpm). (A) Immunofluorescence staining of DRG sections from rats subjected to different treatments, highlighting DAPI (blue), DRP1 (yellow), iNOS (red), ATF-3 (purple), and CGRP (cyan), with IBA1 (green) as a cellular marker. Scale bar = 50 μm. (B) Safranin O/fast green staining of knee joint sections from rats with various treatments. Scale bar = 500 and 100 μm. (C−G) Quantitative analyses of fluorescence areas corresponding to DRP1, iNOS, ATF-3, CGRP, and IBA1, respectively, within the DRG regions. Data are presented as mean ± SD ($n = 9$). *$P < 0.05$, **$P < 0.01$, ***$P < 0.001$, ****$P < 0.0001$. (H) Quantitative assessments of cartilage matrix loss. Data are presented as mean ± SD ($n = 3$). **$P < 0.01$, ***$P < 0.001$, ****$P < 0.0001$. (I) The osteoarthritis research society international (OARSI) grading scale. Data are presented as median ($n = 3$). *$P < 0.05$, **$P < 0.01$.

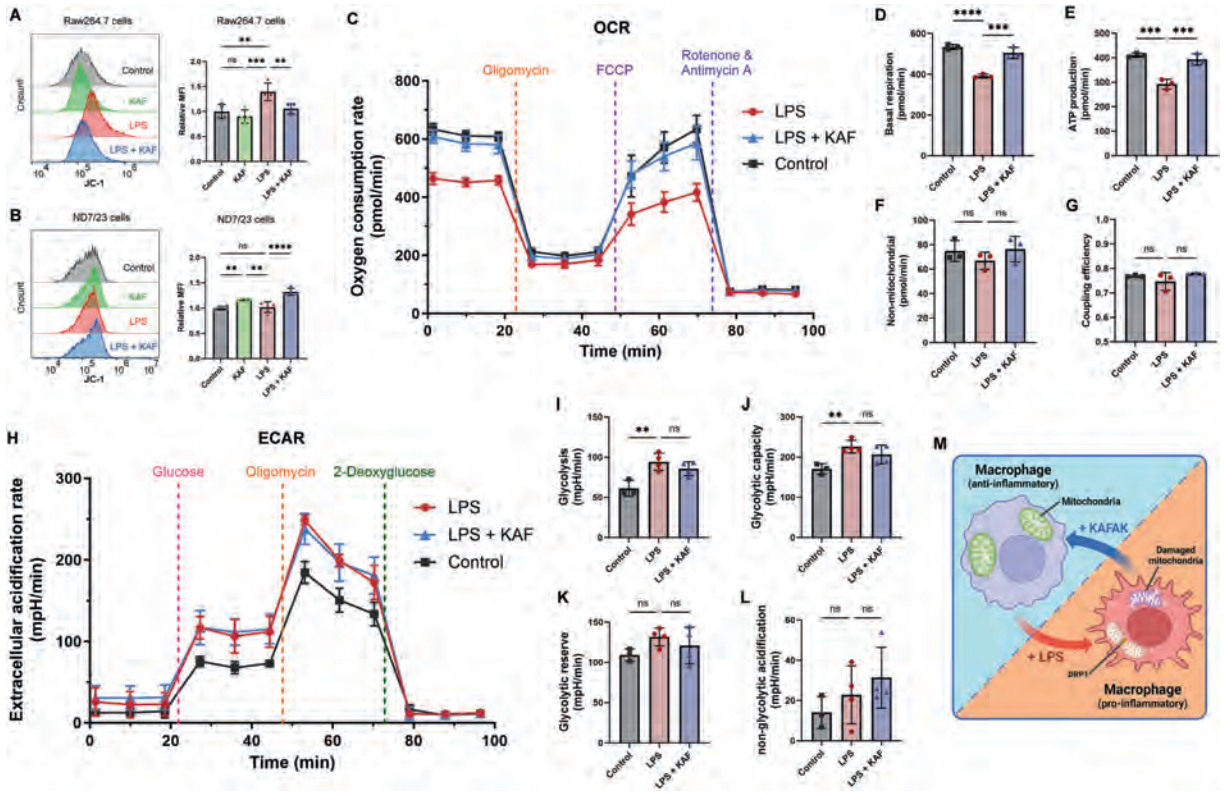

Figure 6 Impact of KAF peptide on mitochondrial function and energy metabolism: (A, B) Flow cytometric analysis of JC-1 staining in Raw264.7 and ND7/23 cells, respectively, following LPS stimulation with or without KAF peptide treatment. Data are presented as mean ± SD ($n = 4$). $^{**}P < 0.01$, $^{***}P < 0.001$, $^{****}P < 0.0001$. ns, not significant. (C) Oxygen consumption rate (OCR) measurements during the Mito Stress Test in Raw264.7 cells, post-treatment with oligomycin, FCCP, and rotenone & Antimycin A. Data are presented as mean ± SD ($n = 3$). (D−G) Comparative analysis of basal respiration, ATP production, non-mitochondrial OCR, and coupling efficiency in LPS-stimulated cells with or without KAF peptide. Data are presented as mean ± SD ($n = 4$). $^{***}P < 0.001$, $^{****}P < 0.0001$. ns, not significant. (H) Extracellular acidification rate (ECAR) profiles following glucose, oligomycin, and 2-DG treatments in the Glycolysis Stress assay. Data are presented as mean ± SD ($n = 4$). (I−L) Comparative assessment of glycolysis, glycolytic capacity, glycolytic reserve, and non-glycolytic acidification in LPS-stimulated cells with or without KAF peptide. Data are presented as mean ± SD ($n = 4$). $^{**}P < 0.01$. ns, not significant. (M) Schematic representation of the role of KAF peptide in modulating macrophage phenotype.

KAF@PLEL hydrogel leverages the thermo-sensitive and biocompatible properties of PLEL to achieve sustained drug release, offering prolonged pain relief. At room temperature, KAF@PLEL remains a liquid, allowing for precise delivery near the DRG. Upon reaching body temperature, it transforms into a gel that encapsulates the DRG, gradually releasing the KAF peptide.

OA chronic pain pathophysiology extends beyond peripheral joint damage and inflammation to encompass central sensitization mechanisms, particularly within the DRG[47]. Solely controlling intra-articular inflammation has limited efficacy in reducing central sensitization. Recent studies have highlighted the significant role of neuroimmune interactions in the development of chronic pain[4,21−24]. Such interactions fundamentally drive the transition from acute to chronic pain.

We strategically employed two complementary OA models: DMM for initial transcriptional profiling and MIA for therapeutic validation. While these models differ in their initial pathogenic triggers-DMM through mechanical destabilization and MIA through metabolic disruption-mechanical destabilization in DMM *versus* metabolic disruption in MIA-they converge on similar pathological endpoints regarding DRG inflammation and pain manifestation. This convergence of findings across models indicates that the observed neuroimmune interactions represent core mechanisms in OA pain pathogenesis rather than model-specific effects. Notably, the patterns of macrophage infiltration and activation in the DRG showed remarkable similarity between the mouse DMM model (evidenced by transcriptional analysis) and our rat MIA model (confirmed through immunofluorescence and functional studies). This cross-species, cross-model validation strengthens the robustness of our findings and their potential therapeutic implications.

We selected the rat MIA model for therapeutic evaluation based on several key advantages. The larger size of rat DRG facilitates more precise para-DRG injection and subsequent tissue analysis, while the relatively faster progression of the MIA model enables more efficient therapeutic assessment. Although the DMM model typically develops over a longer timeframe (weeks to months) compared to MIA (days to weeks), both models ultimately lead to similar chronic pain states characterized by persistent neuroinflammation. This consistent pattern across different models reinforces the therapeutic validity of targeting DRG macrophages for OA pain management, independent of the initial triggering mechanism.

The progression from acute to chronic OA pain intimately relates to metabolic reprogramming in DRG macrophages, specifically in the glycolysis−OXPHOS balance. Pro-

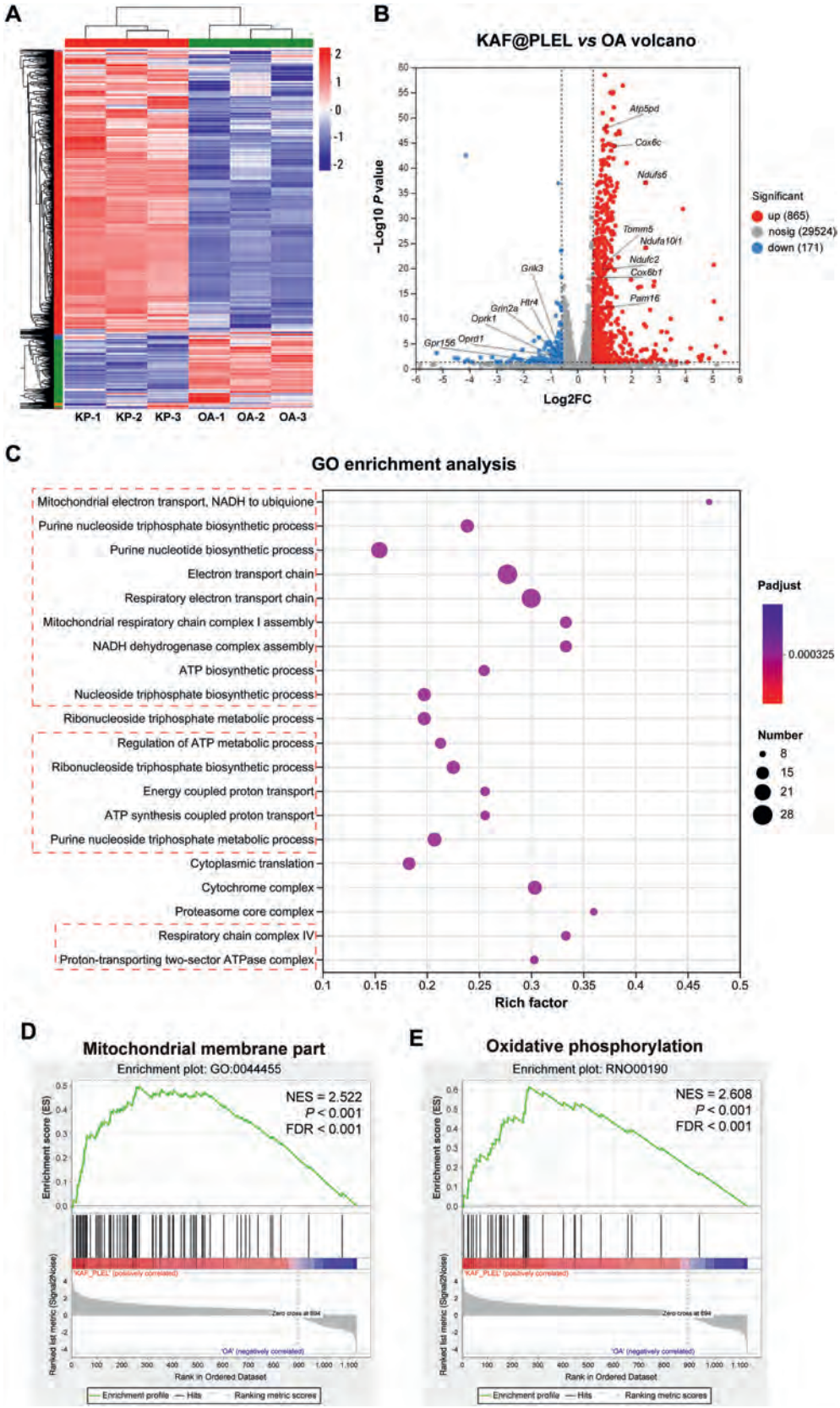

Figure 7 Transcriptomic analysis of DRG in OA rats *versus* KAF@PLEL(KP)-treated OA rats. (A) Heatmap of differentially expressed genes ($n = 3$). (B) Volcano plot depicting gene expression changes (KAF@PLEL *versus* OA; fold change ≥ 1.5; $P < 0.05$). (C) Gene ontology (GO) enrichment analysis of the differentially expressed genes. (D, E) Gene set enrichment analysis (GSEA) of genes associated with mitochondrial membrane and oxidative phosphorylation, respectively, with normalized enrichment score (NES) and false discovery rate (FDR) indicated.

inflammatory (M1) macrophages, which dominate in chronic pain conditions, preferentially utilize glycolysis for their energy needs. This metabolic pathway supports the rapid production of inflammatory mediators, including ROS and pro-inflammatory cytokines, while compromising reduced mitochondrial function[11,48−50].

M1 macrophages exhibit decreased mitochondrial membrane potential, increased expression of DRP1 (which mediates mitochondrial fission), and elevated ROS production[25,51]. Furthermore, OXPHOS decreases M1 macrophages to divert essential substrates toward pro-inflammatory cytokine production from the tricarboxylic acid (TCA) cycle. These changes promote mitochondrial fragmentation and dysfunction, amplifying neuroinflammation and sustaining chronic pain.

Conversely, anti-inflammatory (M2) macrophages rely primarily on OXPHOS for energy, facilitating sustained ATP production and maintaining their anti-inflammatory functions[52]. Efficient OXPHOS critically maintains the M2 phenotype and promotes tissue repair. However, in OA, the mitochondrial impairment observed in DRG macrophages disrupts this balance, favoring a pro-inflammatory state that contributes to ongoing pain.

The KAF@PLEL hydrogel system targets these metabolic disruptions *via* several synergistic mechanisms. At the molecular level, KAF peptide functions *via* direct inhibition of MK2 (MAPKAP kinase 2), an essential downstream mediator of p38 MAPK signaling[46,53,54]. Results from the Seahorse Mito-Stress Test demonstrated that KAF improves OXPHOS and electron transport chain efficiency, thereby counteracting the metabolic shift towards glycolysis that typifies pro-inflammatory macrophages. This metabolic reprogramming simultaneously decreases ROS production and facilitates the transition of macrophages from an M1 to an M2 phenotype. The thermosensitive properties of the PLEL hydrogel enhance this metabolic modulation by enabling precise spatiotemporal control of KAF delivery.

The hydrogel exhibits temperature-dependent behavior stemming from its amphiphilic PEG-PDLLA block architecture. At room temperature, PDLLA segments self-assemble into loose micellar cores while PEG chains extend throughout the aqueous phase, preserving solution fluidity. At physiological temperature, enhanced polymer-polymer interactions drive the formation of a densely crosslinked hydrogel network. This structural reorganization establishes an optimal microenvironment for sustained KAF release while matching DRG tissue mechanics.

Pro-inflammatory macrophage activation near PSNs critically drives chronic pain development, necessitating preserved TCA cycle function and OXPHOS efficiency in resolving chronic OA pain. The dual functionality of our system-integrating targeted drug delivery through the thermosensitive hydrogel with metabolic reprogramming *via* KAF offers a more comprehensive approach to pain management than traditional treatments that address isolated components of OA pain.

This investigation reveals the neuroprotective effects of KAF@PLEL through multiple mechanisms, which complement and surpass current therapeutic approaches. In contrast with traditional injectable hydrogels, such as hyaluronic acid-based systems that mainly offer mechanical support, KAF@PLEL exhibits enhanced biocompatibility and broader therapeutic effects. Recent studies with similar thermosensitive hydrogels have reported cell viability rates of 70%−85%, while our system achieves over 90% cell viability in both nerve and muscle cells under therapeutic conditions. This superior biocompatibility results from the optimized molecular weight distribution and amphiphilic balance of our PLEL copolymer, which reduces cellular stress while preserving effective drug delivery.

The immune-modulating capabilities of KAF@PLEL constitute a significant advance over existing approaches. While previous studies have targeted inflammation through direct cytokine inhibition or broad-spectrum anti-inflammatory agents, our system's ability to reprogram macrophage phenotype offers a longer-lasting solution. Similar immune-modulating biomaterials in tissue engineering applications typically achieve a 20%−30% reduction in pro-inflammatory markers, whereas KAF@PLEL demonstrates approximately a 50% reduction in $CD86^+$ macrophages. This dual action on immune response is especially significant when compared to current clinical treatments for OA pain, which primarily target symptom management rather than resolving underlying immune dysfunction.

Through attenuating the expression of injury markers (ATF-3) and neuropeptides (CGRP) in DRG neurons, the hydrogel safeguarded sensory neurons from further damage and facilitated pain relief. Additionally, KAF@PLEL suppressed microglial activation, suggesting that it can regulate neuroimmune interactions within the DRG, enhancing its analgesic effects.

The translation potential of our system emerges through comparing its performance with current standard-of-care treatments. While conventional treatments like NSAIDs or local anesthetics typically provide pain relief for 24−48 h, our system sustains therapeutic effects for up to three weeks. This extended duration of action parallels recently developed sustained-release formulations that have successfully progressed to clinical trials. Moreover, our ultrasound-guided delivery approach resolves a key limitation of many experimental therapies—the challenge of precise administration to the target tissue. Similar image-guided delivery systems have demonstrated promising results in early-phase clinical trials for various neurological conditions.

Furthermore, primary sensory neurons possess classic pain receptors and immune receptors previously thought to be exclusive to immune cells. This dual receptor expression pattern, newly revealed through single-cell transcriptomics studies, explains why our integrated approach targeting both neural and immune components yields superior outcomes compared to traditional single-target therapies. Upon the stimulation of the production of CGRP neuropeptides by the injury, these receptors subsequently trigger the pain response of neurons and initiate the pro-inflammatory response[55,56]. Consequently, primary sensory neurons can potentially exacerbate pain sensation or local inflammation. Recent research has revealed that primary sensory neurons have complex positive and negative control mechanisms for bone destruction and bone formation[57−59].

These findings highlight the potential of KAF@PLEL as a novel therapeutic approach for chronic OA pain, integrating immune modulation, sustained drug delivery, and precise targeting of affected tissues. While several other hydrogel-based systems for pain management are currently under investigation, our comprehensive mechanistic understanding and robust preclinical data establish KAF@PLEL favorably for future clinical translation. However, additional studies evaluating long-term safety and efficacy in larger animal models remain essential, as similar promising therapies have encountered challenges in late-stage development due to unforeseen safety concerns or diminished efficacy in more complex clinical settings.

The successful development of an ultrasound-guided technique for minimally invasive delivery augments its clinical applicability,

minimizing the need for more invasive procedures. While the study offers promising results, several limitations warrant attention. First, the research utilized animal models, which may not fully mirror the complexities of human OA pain and neuroimmune interactions. Second, the long-term safety and efficacy of KAF@PLEL in clinical settings require further validation. Moreover, the optimal therapeutic concentration of the hydrogel needs further refinement to prevent potential neurotoxicity at higher doses. Lastly, the study did not evaluate potential interactions of KAF@PLEL with existing OA treatments, which could affect its overall effectiveness in a clinical setting. Future studies should resolve these limitations to ensure safe and effective translation to clinical practice.

5. Conclusions

This study presents a novel therapeutic strategy for managing chronic OA pain by specifically modulating neuroimmune interactions within the DRG. The engineered KAF@PLEL hydrogel, optimized for delivering the anti-inflammatory peptide KAF in a sustained-release format, exhibits significant potential in both *in vitro* and *in vivo* models. By orchestrating the transition of DRG macrophages from a pro-inflammatory (M1) to an anti-inflammatory (M2) phenotype, the hydrogel substantially attenuates neuroinflammation, mitigates chronic OA pain, and diminishes nerve and cartilage damage, ultimately resulting in improved motor function in OA rat models. The sustained release properties of the KAF@PLEL hydrogel extend therapeutic effects while reducing systemic exposure, establishing it as a promising alternative to current OA pain treatments. These findings underscore the hydrogel's potential as a targeted and effective treatment for chronic OA pain, targeting central components of pain through neuroimmune modulation.

Acknowledgments

This work was financially supported by the National Natural Science Foundation of China (Nos. U21A20417, 31930067, 82002304, 82301412, 82401456), The 1.3.5 Project for Disciplines of Excellence, West China Hospital, Sichuan University, China (No. ZYJC21068, China), Sichuan Provincial Health Research Projects (No. 2025−111, China), The Young Talents Project of Sichuan Provincial People's Hospital (No. 2022QN50, China), The cadres health research topic Sichuan Province (No. 2023−217, China), The Sichuan Science and Technology Program (No. 2022YFS0439, China).

Author contributions

Yue Liu and Kai Zhou designed the research. Yue Liu, Kai Zhou, Xinlong He, Kun Shi, and Danrong Hu carried out the experiments and performed data analysis. Chenli Yang, Jinrong Peng, Yuqi He, Guoyan Zhao, Yi Kang, Yujun Zhang, Yue'e Dai, Min Zeng, and Feier Xian participated in the experiments. Wensheng Zhang and Zhiyong Qian provided experimental drugs and quality control. Yue Liu and Kai Zhou wrote the manuscript. Wensheng Zhang and Zhiyong Qian revised the manuscript. All of the authors have read and approved the final manuscript.

Conflicts of interest

The authors have no conflicts of interest to declare.

Ethics approval

All procedures were conducted by the ethical guidelines for the care and use of laboratory animals as outlined by the U.S. National Institutes of Health (publication Nos. 80−23, revised in 1996). All experimental procedures were executed according to the protocols approved by the Committee of Animal Care at West China Hospital, Sichuan University, China (approval No. 20230302054).

Data availability statement

Data are available upon reasonable request.

Appendix A. Supporting information

Supporting information to this article can be found online at https://doi.org/10.1016/j.apsb.2025.07.024.

References

1. Leifer VP, Katz JN, Losina E. The burden of OA—health services and economics. *Osteoarthr Cartil* 2021;**30**:10−6.
2. Kloppenburg M, Namane M, Cicuttini F. Osteoarthritis. *Lancet* 2025;**405**:71−85.
3. Allen KD, Thoma LM, Golightly YM. Epidemiology of osteoarthritis. *Osteoarthr Cartil* 2021;**30**:184−95.
4. Raoof R, Martin Gil C, Lafeber FPJG, de Visser H, Prado J, Versteeg S, et al. Dorsal root ganglia macrophages maintain osteoarthritis pain. *J Neurosci* 2021;**41**:8249−61.
5. Mathiessen A, Conaghan PG. Synovitis in osteoarthritis: current understanding with therapeutic implications. *Arthritis Res Ther* 2017;**19**:18.
6. Malfait AM, Schnitzer TJ. Towards a mechanism-based approach to pain management in osteoarthritis. *Nat Rev Rheumatol* 2013;**9**:654−64.
7. Lei Y, Zhang QF, Kuang GZ, Wang XC, Fan QH, Ye FY. Functional biomaterials for osteoarthritis treatment: from research to application. *Smart Med* 2022;**1**:e20220014.
8. Wang QK, Mol MF, Bos PK, Dorleijn DMJ, Vis M, Gussekloo J, et al. Effect of intramuscular *vs* intra-articular glucocorticoid injection on pain among adults with knee osteoarthritis: the KIS randomized clinical trial. *JAMA Netw Open* 2022;**5**:e224852.
9. Laigaard J, Pedersen C, Rønsbo TN, Mathiesen O, Karlsen APH. Minimal clinically important differences in randomised clinical trials on pain management after total hip and knee arthroplasty: a systematic review. *Br J Anaesth* 2021;**126**:1029−37.
10. Rice DA, Kluger MT, McNair PJ, Lewis GN, Somogyi AA, Borotkanics R, et al. Persistent postoperative pain after total knee arthroplasty: a prospective cohort study of potential risk factors. *Br J Anaesth* 2018;**121**:804−12.
11. Sellevold VB, Steindal SA, Lindberg MF, Småstuen MC, Aamodt A, Lerdal A, et al. Many patients with persistent pain 1 year after TKA report improvement by 5 to 7 years: a mixed-methods study. *Clin Orthop Relat Res* 2022;**480**:2075−88.
12. Thakur M, Dickenson AH, Baron R. Osteoarthritis pain: nociceptive or neuropathic. *Nat Rev Rheumatol* 2014;**10**:374−80.
13. Sideris A, Malahias MA, Birch G, Zhong HY, Rotundo V, Like BJ, et al. Identification of biological risk factors for persistent postoperative pain after total knee arthroplasty. *Reg Anesth Pain Med* 2022;**47**:161−6.
14. Felson DT. Mechanisms of osteoarthritis (OA) pain. *Curr Osteoporos Rep* 2018;**16**:611−6.
15. Nijs J, George SZ, Clauw DJ, Fernández-de-Las-Peñas C, Kosek E, Ickmans K, et al. Central sensitisation in chronic pain conditions:

latest discoveries and their potential for precision medicine. *Lancet Rheumatol* 2021;**3**:e383−92.
16. Zolio L, Lim KY, McKenzie JE, Yan MK, Estee M, Hussain SM, et al. Systematic review and meta-analysis of the prevalence of neuropathic-like pain and/or pain sensitization in people with knee and hip osteoarthritis. *Osteoarthr Cartil* 2021;**29**:1096−116.
17. Kratter C. Therapeutic management of the painful nerve: a narrative review of common rehabilitation interventions. *Plast Aesthet Res* 2024;**11**:1.
18. Di Valerio E, Lautenslager L, Vonu P, Mustafa C, Chim H, Satteson E. Efficacy of targeted muscle reinnervation for treating and preventing postamputation pain—a systematic review. *Plast Aesthet Res* 2022;**9**: 62.
19. Kupari J, Usoskin D, Parisien M, Lou DH, Hu YZ, Fatt M, et al. Single cell transcriptomics of primate sensory neurons identifies cell types associated with chronic pain. *Nat Commun* 2021;**12**:1510.
20. Yu XB, Basbaum A, Guan ZH. Contribution of colony-stimulating factor 1 to neuropathic pain. *Pain Rep* 2021;**6**:e883.
21. Ji RR, Chamessian A, Zhang YQ. Pain regulation by non-neuronal cells and inflammation. *Science* 2016;**354**:572−7.
22. Raoof R, Willemen HLDM, Eijkelkamp N. Divergent roles of immune cells and their mediators in pain. *Rheumatology* 2018;**57**:429−40.
23. Martin Gil C, Raoof R, Versteeg S, Willemen HLDM, Lafeber FPJG, Mastbergen SC, et al. Myostatin and CXCL11 promote nervous tissue macrophages to maintain osteoarthritis pain. *Brain Behav Immun* 2024;**116**:203−15.
24. Geraghty T, Winter DR, Miller RJ, Miller RE, Malfait AM. Neuro-immune interactions and osteoarthritis pain: focus on macrophages. *Pain Rep* 2021;**6**:e892.
25. Marchi S, Guilbaud E, Tait SWG, Yamazaki T, Galluzzi L. Mitochondrial control of inflammation. *Nat Rev Immunol* 2023;**23**:159−73.
26. Yanamadala Y, Roy R, Williams AA, Uppu N, Kim AY, DeCoster MA, et al. Intranasal delivery of cell-penetrating therapeutic peptide enhances brain delivery, reduces inflammation, and improves neurologic function in moderate traumatic brain injury. *Pharmaceutics* 2024;**16**:774.
27. Biji CA, Balde A, Abdul Nazeer R. Anti-inflammatory peptide therapeutics and the role of sulphur containing amino acids (cysteine and methionine) in inflammation suppression: a review. *Inflamm Res* 2024; **73**:1203−21.
28. Li X, Dai BY, Guo JX, Zheng LZ, Guo QY, Peng J, et al. Nanoparticle-cartilage interaction: pathology-based intra-articular drug delivery for osteoarthritis therapy. *Nano-Micro Lett* 2021;**13**:149.
29. Zhou K, Yang CL, Shi K, Liu Y, Hu DR, He XL, et al. Activated macrophage membrane-coated nanoparticles relieve osteoarthritis-induced synovitis and joint damage. *Biomaterials* 2023;**295**:122036.
30. Li Q, Wang ZZ, Shi N, Qi Y, Yao WF, Yu J, et al. Application and prospect of the therapeutic strategy of inhibiting cellular senescence combined with pro-regenerative biomaterials in regenerative medicine. *Smart Med* 2023;**2**:e20230030.
31. Chen W, Shi K, Liu J, Yang PP, Han RX, Pan M, et al. Sustained co-delivery of 5-fluorouracil and cis-platinum *via* biodegradable thermosensitive hydrogel for intraoperative synergistic combination chemotherapy of gastric cancer. *Bioact Mater* 2022;**23**:1−15.
32. Liu J, Yang TY, Dai LQ, Shi K, Hao Y, Chu BY, et al. Intravesical chemotherapy synergize with an immune adjuvant by a thermosensitive hydrogel system for bladder cancer. *Bioact Mater* 2023;**31**: 315−32.
33. Zhang YJ, Shi K, Yang X, Chen W, Wang TH, Kang Y, et al. Sustained release of levobupivacaine from temperature-sensitive injectable hydrogel for long-term local anesthesia in postoperative pain management. *Biomaterials* 2023;**299**:122129.
34. Yuan XM, Han SY, Zhao FT, Manyande A, Gao F, Wang J, et al. Rapid injection of lumbar dorsal root ganglia under direct vision: relevant anatomy, protocol, and behaviors. *Front Neurol* 2023;**14**:1138933.
35. Comi E, Lanza M, Ferrari F, Mauri V, Caselli G, Rovati LC. Efficacy of CR4056, a first-in-class imidazoline-2 analgesic drug, in comparison with naproxen in two rat models of osteoarthritis. *J Pain Res* 2017;**10**:1033−43.
36. Ishikawa G, Koya Y, Tanaka H, Nagakura Y. Long-term analgesic effect of a single dose of anti-NGF antibody on pain during motion without notable suppression of joint edema and lesion in a rat model of osteoarthritis. *Osteoarthr Cartil* 2015;**23**:925−32.
37. Padera RF, Tse JY, Bellas E, Kohane DS. Tetrodotoxin for prolonged local anesthesia with minimal myotoxicity. *Muscle Nerve* 2006;**34**:747−53.
38. Yin QQ, Zhang YJ, Lv R, Gong DY, Ke BW, Yang J, et al. A fixed-dose combination, QXOH/levobupivacaine, produces long-acting local anesthesia in rats without additional toxicity. *Front Pharmacol* 2019;**10**:243.
39. Park EH, Seo J, Lee Y, Park K, Kim KR, Kim S, et al. TissueGene-C induces long-term analgesic effects through regulation of pain mediators and neuronal sensitization in a rat monoiodoacetate-induced model of osteoarthritis pain. *Osteoarthr Cartil* 2023;**31**:1567−80.
40. Abdelhamid MS, El Bohi KM, Sherif MH, Abdelhamid MS, Abdel-Daim MM, Elewa YHA, et al. Apitoxin alleviates methyl mercury-induced peripheral neurotoxicity in male rats by regulating dorsal root ganglia neuronal degeneration and oxidative stress. *Biomed Pharmacother* 2023;**161**:114521.
41. Conaghan PG, Cook AD, Hamilton JA, Tak PP. Therapeutic options for targeting inflammatory osteoarthritis pain. *Nat Rev Rheumatol* 2019;**15**:355−63.
42. Desai N, Kirkham KR, Albrecht E. Local anaesthetic adjuncts for peripheral regional anaesthesia: a narrative review. *Anaesthesia* 2021; **76**:100−9.
43. Fowler MJ, Cotter JD, Knight BE, Sevick-Muraca EM, Sandberg DI, Sirianni RW, et al. Intrathecal drug delivery in the era of nanomedicine. *Adv Drug Deliv Rev* 2020;**165**:77−95.
44. Kim H, Na DL, Lee NK, Kim AR, Lee S, Jang H, et al. Intrathecal injection in a rat model: a potential route to deliver human Wharton's jelly-derived mesenchymal stem cells into the brain. *Int J Mol Sci* 2020;**21**:1272.
45. Rahman MM, Lee JY, Kim YH, Park CK. Epidural and intrathecal drug delivery in rats and mice for experimental research: fundamental concepts, techniques, precaution, and application. *Biomedicines* 2023; **11**:1413.
46. Yu GL, Segel I, Zhang ZY, Hogan QH, Pan B. Dorsal root ganglion stimulation alleviates pain-related behaviors in rats with nerve injury and osteoarthritis. *Anesthesiology* 2020;**133**:408−25.
47. Lee GI, Neumeister MW. Pain: pathways and physiology. *Clin Plast Surg* 2020;**47**:173−80.
48. Palmieri EM, Gonzalez-Cotto M, Baseler WA, Davies LC, Ghesquière B, Maio N, et al. Nitric oxide orchestrates metabolic rewiring in M1 macrophages by targeting aconitase 2 and pyruvate dehydrogenase. *Nat Commun* 2020;**11**:698.
49. Gupta S, Sarangi PP. Inflammation driven metabolic regulation and adaptation in macrophages. *Clin Immunol* 2022;**246**:109216.
50. Kolliniati O, Ieronymaki E, Vergadi E, Tsatsanis C. Metabolic regulation of macrophage activation. *J Innate Immun* 2022;**14**:51−68.
51. Billingham LK, Stoolman JS, Vasan K, Rodriguez AE, Poor TA, Szibor M, et al. Mitochondrial electron transport chain is necessary for NLRP3 inflammasome activation. *Nat Immunol* 2022;**23**:692−704.
52. Devanney NA, Stewart AN, Gensel JC. Microglia and macrophage metabolism in CNS injury and disease: the role of immunometabolism in neurodegeneration and neurotrauma. *Exp Neurol* 2020;**329**:113310.
53. Li T, Yang JJ, Weng CM, Liu PJ, Huang Y, Meng S, et al. Intra-articular injection of anti-inflammatory peptide-loaded glycol chitosan/fucoidan nanogels to inhibit inflammation and attenuate osteoarthritis progression. *Int J Biol Macromol* 2021;**170**:469−78.
54. Song YZ, Zhang T, Cheng HG, Jiang W, Li P, Zhang J, et al. Imidazolium-based ionic liquid-assisted preparation of nano-spheres loaded with bio-active peptides to decrease inflammation in an osteoarthritis model: *ex vivo* evaluations. *J Biomed Nanotechnol* 2021;**17**: 859−72.

55. Maruyama K. Senso-immunology: crosstalk between nociceptive and immune systems. *FEBS J* 2022;**289**:4132−45.
56. Baral P, Udit S, Chiu IM. Pain and immunity: implications for host defence. *Nat Rev Immunol* 2019;**19**:433−47.
57. Miyamoto S, Takayama Y, Kondo T, Maruyama K. Senso-immunology: the hidden relationship between sensory system and immune system. *J Bone Miner Metabol* 2024;**42**:413−20.
58. Gao F, Hu QM, Chen WW, Li JL, Qi C, Yan YW, et al. Brain regulates weight bearing bone through PGE2 skeletal interoception: implication of ankle osteoarthritis and pain. *Bone Res.* 2024;**12**:16.
59. Li JQ, Liu B, Wu H, Zhang SS, Liang ZW, Guo S, et al. Sensory nerves directly promote osteoclastogenesis by secreting peptidylprolyl cis-trans isomerase D (Cyp40). *Bone Res.* 2023;**11**:64.